AMERICAN SOCIETY FOR MICROBIOLOGY | Antimicrobial Agents and Chemotherapy

Zinc(II)-Dipicolylamine Coordination Complexes as Targeting and Chemotherapeutic Agents for *Leishmania major*

Douglas R. Rice,[a] Paola Vacchina,[b] Brianna Norris-Mullins,[b] Miguel A. Morales,[b] Bradley D. Smith[a]

Department of Chemistry and Biochemistry, University of Notre Dame, Notre Dame, Indiana, USA[a]; Eck Institute for Global Health, Department of Biological Sciences, University of Notre Dame, Notre Dame, Indiana, USA[b]

Cutaneous leishmaniasis is a neglected tropical disease that causes painful lesions and severe disfigurement. Modern treatment relies on a few chemotherapeutics with serious limitations, and there is a need for more effective alternatives. This study describes the selective targeting of zinc(II)-dipicolylamine (ZnDPA) coordination complexes toward *Leishmania major*, one of the species responsible for cutaneous leishmaniasis. Fluorescence microscopy of *L. major* promastigotes treated with a fluorescently labeled ZnDPA probe indicated rapid accumulation of the probe within the axenic promastigote cytosol. The antileishmanial activities of eight ZnDPA complexes were measured using an *in vitro* assay. All tested complexes exhibited selective toxicity against *L. major* axenic promastigotes, with 50% effective concentration values in the range of 12.7 to 0.3 μM. Similar toxicity was observed against intracellular amastigotes, but there was almost no effect on the viability of mammalian cells, including mouse peritoneal macrophages. *In vivo* treatment efficacy studies used fluorescence imaging to noninvasively monitor changes in the red fluorescence produced by an infection of mCherry-*L. major* in a mouse model. A ZnDPA treatment regimen reduced the parasite burden nearly as well as the reference care agent, potassium antimony(III) tartrate, and with less necrosis in the local host tissue. The results demonstrate that ZnDPA coordination complexes are a promising new class of antileishmanial agents with potential for clinical translation.

Leishmaniasis is a parasite infection transmitted to mammals by the bites of infected female phlebotomine sandflies. It is endemic in more than 70 countries worldwide, with approximately 12 million people infected and 310 million at risk of infection (1). The disease is associated with impoverished areas of the Middle East, Southeast Asia, and South America. Different *Leishmania* species are responsible for the two main disease manifestations: visceral and cutaneous. The visceral form mainly targets the liver and spleen resulting in high-grade fever and organ failure. It is the most lethal form and the second greatest parasitic killer in the world (2). The cutaneous form is an infection of the dermis which produces inflamed lesions that heal slowly, leaving scars, or that can evolve into mucosal infections which cause oral, nasal, and pharyngeal tissue damage (3). Consequently, patients can suffer devastating facial disfigurement and aesthetic trauma.

Modern treatment regimens for cutaneous infections involve local application of antimonial drugs, such as meglumine antimoniate and sodium stibogluconate (4). Antimonial based therapies have been the primary treatment option since their development in the early 1930s (5). These drugs are notable as pioneering therapeutics, but they exhibit numerous drawbacks. Antimonials are generally expensive, nonspecific, and toxic to internal organs. Routine doses cause painful side effects such as vomiting, swelling, and myalgia (5). Additionally, antimonial therapy is prohibited in many patient populations such as women during pregnancy, young children, and patients suffering from chronic conditions such as kidney disease or heart failure (6). Antifungal- and antibiotic-based drugs such as amphotericin B, paromomycin, and pentamidine isethionate are second-line treatments, but severe side effects and high cost limit their use (4, 7). Anticancer agents such as miltefosine are promising but relatively expensive, potentially teratogenic, and prone to result in infection relapse after treatment (8). Taken together, the weaknesses of existing remedies highlight the need for new classes of effective, nontoxic, and inexpensive antileishmanial chemotherapeutics.

Cationic molecules are attractive starting points for *Leishmania* drug discovery because they can distinguish the anionic surface charge of the parasites from the near-neutral membrane surface charge of healthy mammalian host cells. *Leishmania* parasites are negatively charged due to (i) a thick coating of the anionic polysaccharide lipophosphoglycan, which covers ~60% of the parasite surface, and (ii) a high fraction of anionic polar lipids within the plasma membrane (9–13). Certain classes of cationic peptides and cationic liposomes bearing sterylamine are toxic to *Leishmania* (14–16). In addition, aromatic dicationic compounds structurally related to pentamidine are active against *L. infantum* (17), and the positively charged small molecule sitamaquine has undergone phase II clinical trials for treatment of visceral infections (18). The toxic mechanisms of these treatments are not well understood, but they appear to occur through a combination of factors, including membrane depolarization, mitochondrial disruption, or DNA damage.

The present study evaluates a series of cationic zinc(II)-dipicolylamine (ZnDPA) coordination complexes for ability to selec-

Received 19 February 2016 **Accepted** 25 February 2016

Accepted manuscript posted online 29 February 2016

Citation Rice DR, Vacchina P, Norris-Mullins B, Morales MA, Smith BD. 2016. Zinc(II)-dipicolylamine coordination complexes as targeting and chemotherapeutic agents for *Leishmania major*. Antimicrob Agents Chemother 60:2932–2940. doi:10.1128/AAC.00410-16.

Address correspondence to Bradley D. Smith, smith.115@nd.edu, or Miguel A. Morales, miguel.morales@nd.edu.

Supplemental material for this article may be found at http://dx.doi.org/10.1128/AAC.00410-16.

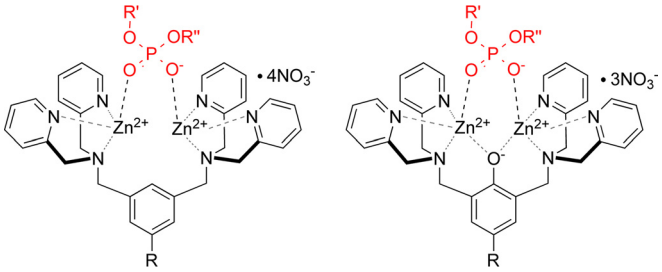

FIG 1 Association of ZnDPA coordination complexes with phosphorylated amphiphiles on the cell surface.

tively target and kill *Leishmania* parasites. ZnDPA complexes are known to selectively recognize anionic cell surfaces due to a combination of general electrostatic attraction and specific coordination of the zinc cations with the phosphate and carboxylate groups on the polar lipids in the cell membrane (Fig. 1). Fluorescent ZnDPA probes are effective imaging agents for dead and dying mammalian cells (which expose anionic phosphatidylserine) in a range of cell culture systems and small animal models of disease (19–26). ZnDPA probes also target the anionic surfaces of bacteria, and they have been used for imaging infection in animal models (27–33). Some ZnDPA complexes are known to have antibiotic activity due to their capacity to disrupt bacterial membranes (31).

The objective of this study was to determine whether ZnDPA complexes can selectively target *L. major*, a common species responsible for most cutaneous leishmaniasis infections in the Middle East and North Africa (34). A fluorescently labeled ZnDPA probe was used for promastigote staining experiments, and a library of eight ZnDPA complexes was evaluated for *in vitro* toxicity against *L. major* promastigotes, amastigotes, and mammalian cells. A chemotherapeutic candidate was chosen for further activity testing against intracellular amastigotes, murine macrophages, and a mouse model of cutaneous leishmaniasis. To facilitate measurements of *in vivo* efficacy, a fluorescence imaging method was developed using a genetically modified *L. major* strain that expressed the red fluorescent protein mCherry. A mouse footpad infection model enabled direct comparison of treatment efficacy for a ZnDPA complex and a standard antimonial chemotherapeutic agent.

MATERIALS AND METHODS

Materials. The targeted fluorescent ZnDPA probe mSeek, nontargeted fluorescent Control Dye, and all ZnDPA complexes tested were synthesized as previously reported (22, 33). Microscopy slides and coverslips were purchased from Thermo Scientific. Unless otherwise stated, all reagents and solvents were purchased from Sigma-Aldrich.

***Leishmania* culture conditions.** *Leishmania major* axenic promastigotes (MHOM/JL/80/Friedlin), a fluorescent transgenic *L. major* strain constitutively expressing mCherry (mCherry-*L. major*), and a fluorescent transgenic strain of mCherry-*L. donovani* axenic amastigotes were maintained at 27°C in M199 medium supplemented with 10% fetal bovine serum (FBS; Atlanta Biolabs) (35).

***In vitro* toxicity assay and EC_{50} calculation.** Toxicity against *L. major* promastigotes and intracellular amastigotes was assessed using the fluorometric resazurin-based method CellTiter-Blue (Promega) as previously described (35). For promastigotes, 10^6 cells/ml were seeded in a 96-well plate and incubated in the presence of increasing concentrations of ZnDPA complex for 72 h at 27°C, along with the appropriate solvent controls. Afterward, 20 μl of CellTiter-Blue reagent was added to 100 μl of the cell culture, followed by a 4-h incubation period at 37°C, and the fluorescence was measured (excitation, 555 nm; emission, 580 nm) using a Typhoon FLA 9500 laser scanner (GE Healthcare) and analyzed with ImageQuant TL software (GE Healthcare). The output fluorescence values were background subtracted from wells containing medium alone and normalized to wells containing untreated *L. major*. Normalized fluorescence values were plotted against the ZnDPA complex concentration using GraphPad Prism 5 software and fitted to the following curve to determine the 50% effective concentration (EC_{50}):

$$y = a \times \frac{b - a}{\left[1 \times \left(x/c\right)^{d}\right]} \quad (1)$$

where a is the estimated bottom of the curve, b is the estimated top of the curve, c is the 50% effective concentration (EC_{50}), and d is the Hill coefficient.

L. major intracellular amastigote viability was evaluated using a back-differentiation method with RAW264.7 murine macrophages and infective-stage mCherry parasites (36). Briefly, 10^6 metacyclic promastigotes/ml were added to wells in a 96-well plate seeded with 10^5 macrophages/ml. The infection was performed over 8 h in RPMI 1640 medium at a multiplicity of infection of 10 metacyclic parasites per macrophage (10:1). Free parasites were removed by one wash with RPMI 1640 medium. At 24 h postinfection, ZnDPA compound 7 was added in increasing concentrations and incubated for 48 h at 37°C, followed by a 12 h of incubation at 26°C to facilitate back differentiation from viable amastigotes to promastigotes. To detect the remaining viable parasites, 30 μl of CellTiter-Blue reagent were incubated for 4 h with 200 μl of culture at 37°C, followed by a fluorescence measurement and sample analysis as described above. Each assay was performed in triplicate.

Mammalian cell culture and toxicity. CHO-K1 (Chinese hamster ovary) cells, purchased from the American Type Culture Collection (CCL-61), were spread into 96-microwell plates and grown to confluence of 85% in RPMI or F-12K media supplemented with 10% FBS and 1% streptavidin L-glutamate at 37°C and 5% CO_2. CHO cell viability was measured by using a 3-(4,5-dimethylthiazol-2-yl)-2,5-diphenyltetrazolium bromide (MTT) cell viability assay. The number of living cells is directly correlated to the amount of reduced MTT, which is monitored by absorbance at 570 nm. Only active reductase enzymes in viable cells can perform the reduction reaction. A Vybrant MTT cell proliferation assay (Invitrogen, Eugene, OR) was performed according to the manufacturer's protocol. The CHO cells were treated with incremental concentrations of a ZnDPA complex (0 to 50 μM) and incubated for 24 h at 37°C. The medium was replaced with 100 μl of F-12K medium containing MTT (1.2 mM) and incubated at 37°C and 5% CO_2 for an additional 4 h. An SDS-HCl detergent solution was added, and the absorbance of each well was read at 570 nm and normalized to wells containing cells but no added ZnDPA complex ($n = 3$).

Host cell viability was tested using macrophages isolated from the intraperitoneal cavities of three BALB/c mice. Using an insulin syringe with a 24-gauge needle, 5-ml aliquots of Dulbecco modified Eagle medium (DMEM; Life Technologies) supplemented with 10% FBS were injected and then extracted from the peritoneal cavities of euthanized mice. The fluid was centrifuged, and the supernatant was discarded. The pelleted macrophage cells were used to seed 10^5 macrophage/ml in a 96-well plate and incubated in the presence of increasing concentrations of ZnDPA compound 7 for 48 h at 37°C in the presence of 5% CO_2. Viability was measured with the Cell-Titer Blue assay as described above.

Promastigote and amastigote fluorescence microscopy. Samples of mCherry-*L. major* axenic promastigotes and mCherry-*L. donovani* axenic amastigotes (10^7/ml) were fixed with 1% formalin in 1.5-ml microcentrifuge tubes, followed by centrifugation (3,000 rpm, 5 min). The fixed parasites were resuspended in 1 ml of sterile phosphate-buffered saline (145 mM NaCl [pH 7.4]) and treated for 15 min with green-emitting fluorescent ZnDPA probe mSeek (5 to 10 μM) and two drops of NucBlue Fixed Cell ReadyProbes reagent (Thermo Fisher). The samples were washed

twice with fresh buffer to reduce background fluorescence, dispersed into solution, and then placed on slides coated with L-lysine. Preliminary micrographs of promastigotes were acquired using a Nikon Eclipse TE2000-U epifluorescence microscope with a 60× objective and a Photometrics Cascade 512B CCD. Fluorescence images were captured using UV (excitation, 340/80 nm; emission, 435/85 nm), GFP (450/90, 500/50), and Cy3 (535/50, 610/75) filter sets. Micrographs of amastigotes were acquired using an Applied Precision DeltaVision OMX epifluorescence microscope with a 63× objective and similar filter sets.

Confocal scanning laser microscopy of mCherry-*L. major* promastigotes was performed using a Nikon A1R confocal microscope to examine the cellular localization of mSeek. Cell staining was carried out using the procedure above. Twenty sequential planar images were taken over a 2-μm Z-scan range (0.1 μm apart) using a 60× microscope objective and blue, red, and green wavelength filters. The internalization of mSeek within macrophages was evaluated using RAW264.7 murine macrophages. Briefly, mSeek (10 μM) was added to a single well in a six-well plate seeded with 10^5 macrophages/ml, followed by incubation for 24 h at 37°C. Fluorescence microscopy was performed using a Nikon Eclipse TE2000-U epifluorescence microscope with a 40× objective and a Photometrics Cascade 512B CCD. Fluorescence images were captured using the GFP (450/90, 500/50) and Cy3 (535/50, 610/75) filter sets.

Promastigote flow cytometry. Fixed *L. major* axenic promastigotes were stained with Control Dye or mSeek (5 μM final concentration) suspended in sterile phosphate-buffered saline for 10 min at 25°C, followed by three additional wash steps. The samples were injected into a Beckman FC-500 flow cytometer equipped with a Biosense flow cell and a 6-W argon ion laser. The excitation laser was tuned for an 480-nm emission (500 mW), and the emission light was measured using a 530-nm pass absorbance filter. Histograms were generated using FlowJo IX software and represent a total of 50,000 to 100,000 events each. Fluorescence and count data were normalized to "polychromatic" calibration beads.

Fluorescence imaging of cutaneous leishmaniasis in mouse footpad. All animal experiments used protocols that were approved by the Notre Dame Institutional Animal Care and Use Committee (IACUC no. 15-10-2708). Stationary mCherry-*L. major* promastigotes were resuspended in fresh M199 media. Cohorts of BALB/c mice (female, 4 weeks old, Charles River Laboratories) were transferred to a sterile hood. Each mouse was anesthetized with isoflurane, followed by skin sterilization with 70% ethanol and a subcutaneous injection of 10^8 parasites into the left hind footpad. Two weeks later, the mice were anesthetized and subjected to planar fluorescence imaging using an IVIS Lumina (Xenogen) equipped with a 150-W quartz tungsten halogen 21-V bulb for excitation with the following fluorescence acquisition parameters: DsRed fluorescence (excitation, 500 to 550 nm; emission, 575 to 650 nm); acquisition time, 3 s; binning, 2×2; F-stop, 2; and field-of-view, 10 by 10 cm. After imaging, footpad thickness (lesion size) was measured using a Vernier caliper, and the infected footpad was photographed using a Canon PowerShot 12.1 MP digital camera. The 16-bit TIFF images of each living mouse at the different time points were sequentially opened using the ImageJ 1.40g software. The images were cropped to focus only on the infected footpad and then converted to an image stack using the "convert images to stack" software command. The stack of images was background subtracted using the rolling ball algorithm (radius, 250 pixels). Next, the image stack was set to the "Fire" fluorescence intensity scale (under the "Lookup Tables" menu) which color-codes the fluorescence counts contained in each pixel. The stack of images was converted into a montage using the "Convert Stack to Montage" command. A calibration bar was added to the montage using the "Calibration Bar" command, and the resulting image was saved as a TIFF file. Infection burden was quantified by the measuring the mean pixel intensity within a region of interest drawn around each infected footpad. After each time point, a cohort of mice ($n = 4$) were sacrificed, and the infected footpads were harvested to measure parasite burden using the limiting dilution method.

Quantification of parasite burden in mouse footpad. The following procedure was adapted a previously published method (37). Infected footpads were removed by severing the mouse ankle just above the bridge of the foot with surgical scissors. Severed footpads were sterilized with 70% ethanol and placed in a Falcon tube submerged in ice water containing 5 ml of chilled DMEM. The footpads were taken to a sterile culture hood, sliced into small pieces using a disposable scalpel within a sterile petri dish, and homogenized in the original DMEM buffer using a glass/Teflon homogenizer (Thomas Scientific). A 500-μl aliquot of the homogenized footpad solution was serially diluted in a 12-well plate with eight wells containing 4.5 ml of M199 medium per well. Finally, 100 μl from each 12-well plate was dispensed into a separate marked row of a 96-well plate and placed into a 27°C incubator for 5 to 10 days ($n = 3$). After cloudiness developed within the wells, indicating parasite growth, a microscopic evaluation using an Amscope B10 binocular biological microscope was performed to determine the numbers of *Leishmania*-positive and *Leishmania*-negative wells. The parasite load in the mouse footpad was determined from serial dilution calculations.

Treatment of cutaneous leishmaniasis in mouse footpad. Sixteen BALB/c mice were inoculated with mCherry-*L. major* as described above and allowed to form an infection over a 14-day period. After infection, the mice were separated into cohorts of four and administered one of the following treatment regimens: saline (150 mM NaCl, five doses/week), antimonial [5.5 mM potassium antimony(III) tartrate, five doses/week], or ZnDPA compound 7 (see Fig. 3, 80 μM) at a frequency of two or five doses per week. All treatments were 30-μl intralesional injections of agent dissolved in sterile saline (pH 7.4) and administered after the skin was sterilized with a 70% ethanol wipe. The injections were administered at different sites around the lesion to reduce injury from the needle puncture and to spread treatment throughout the infected footpad. Planar fluorescence imaging of each cohort was performed periodically throughout the 12-day treatment period using the following acquisition parameters: DsRed fluorescence (excitation, 500 to 550 nm; emission, 575 to 650 nm); acquisition time, 4 s; binning, 2×2; F-stop, 2; and field-of-view, 10 by 10 cm. After treatment, the mice were sacrificed, and the infected footpads were harvested to measure parasite burden using the limiting dilution method described above ($n = 3$, one mouse was euthanized before the treatment ended).

Histology. Separate cohorts of uninfected BALB/c ($n = 3$) were given intradermal footpad injections of saline or ZnDPA compound 7 at a frequency of five doses per week for 2 weeks as described above. After the treatment period, the mice were euthanized, and the treated footpads were excised, fixed, and then embedded and flash frozen in OCT (Tissue-Tek). Footpad tissue was sliced (8-μm thickness) at −17°C, and the slices adhered to Unifrost microscope slides (Azer Scientific, USA); they were then fixed with chilled acetone for 10 min and air dried for an additional 20 min. Tissue sections were stained with hematoxylin-eosin and imaged using a Nikon 90i upright/widefield equipped with a ×40 objective lens and color camera.

RESULTS

Fluorescence microscopy studies. Selective targeting of a ZnDPA complex to axenic promastigotes and amastigotes was assessed using fluorescence microscopy and flow cytometry. The studies used mCherry-*L. major* promastigotes and mCherry-*L. donovani* axenic amastigotes, which stably expressed the red fluorescent mCherry protein (excitation, 587 nm; emission, 610 nm) in the cytoplasm (see Fig. S1 in the supplemental material) (38). *L. donovani* axenic amastigotes were studied because there are no current methods for culturing *L. major* axenic amastigotes. The parasites were fixed with 1% formalin prior to imaging to ensure membrane integrity and arrest cellular mobility for high-resolution fluorescence micrographs. Aliquots of parasites were incubated with mSeek, a green-emitting fluorescent ZnDPA probe

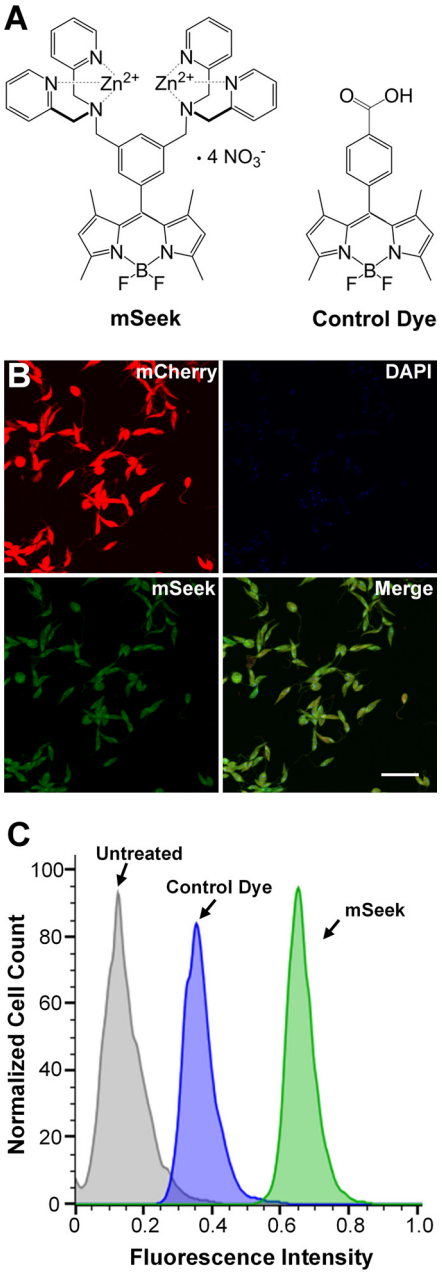

FIG 2 (A) Structures of green-emitting fluorescent ZnDPA probe mSeek and control dye (B) Confocal micrographs of fixed mCherry-*L. major* promastigotes stained with DAPI (4′,6′-diamidino-2-phenylindole) and mSeek (5 μM) for 10 min prior to red, blue, and green fluorescence imaging. The montage is slice 10 (×60 magnification) from a series of 20 slices acquired through a 2-μm Z-scan range (0.1 μm between each slice). (C) Representative flow cytometry histograms of *L. major* cells with green fluorescence ($n = 3$).

(Fig. 2A) for 10 min prior to three wash steps. The treated parasites were first examined using widefield fluorescence microscopy, which revealed strong and uniform staining by the mSeek throughout the parasites, including the promastigote flagellum (see Fig. S2 and S3 in the supplemental material). Additional samples of probe stained promastigotes were imaged with a confocal microscope, which permitted three-dimensional fluorescence imaging. Confocal micrographs of the parasite interior showed

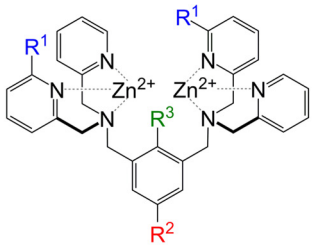

ZnDPA	R^1	R^2	R^3	EC_{50} (μM)
1	H	H	H	4.1 ± 0.4
2	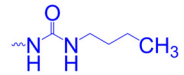	H	H	0.7 ± 0.3
3	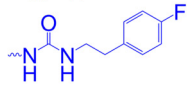	H	H	1.1 ± 0.2
4	H	$O(CH_2)_4NH_2$	H	3.2 ± 0.8
5	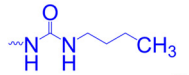	$O(CH_2)_4NH_2$	H	1.7 ± 0.4
6	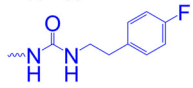	$O(CH)_4NH_2$	H	0.3 ± 0.1
7	H	CH_3	O^-	2.3 ± 0.2
8	H	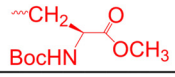	O^-	12.7 ± 1.2

FIG 3 Structures of ZnDPA complexes tested for *L. major* toxicity and EC_{50} values.

clearly that the mSeek was dispersed throughout the cytoplasm colocalizing with cytoplasmic mCherry (Fig. 2B). The microscopy showed negligible promastigote staining by the nontargeted Control Dye that lacked a ZnDPA complex. In addition, flow cytometry histograms of parasites treated with mSeek indicated ~3-fold-higher fluorescence than parasites treated with Control Dye (Fig. 2C). To determine macrophage uptake, murine macrophages were incubated for 24 h with mSeek, followed by fluorescence microscopy. The probe fluorescence was dispersed throughout the macrophage cytoplasm, with noticeably higher intensity than the background macrophage autofluorescence (see Fig. S4 in the supplemental material).

TABLE 1 *In vitro* activity of ZnDPA (compound 7) against mammalian cells and *L. major* promastigotes and amastigotes

Evaluation model and cell type	Mean EC_{50} (μM) ± SD[a]
Cellular evaluation	
CHO-K1	>50
Peritoneal macrophages	>10
Parasite evaluation	
Axenic promastigotes	2.3 ± 0.2
Intracellular amastigotes	4.7 ± 0.1

[a] For at least three replicates.

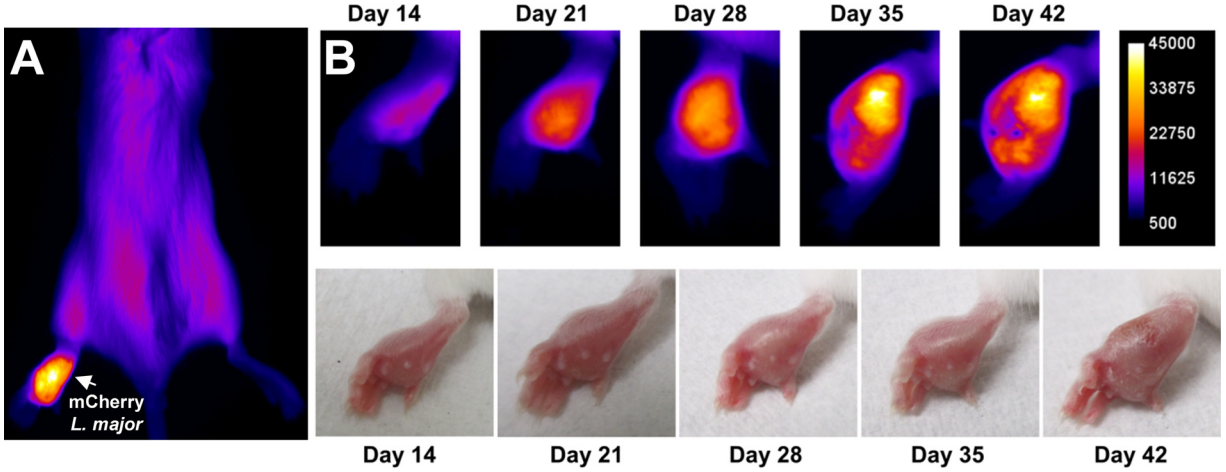

FIG 4 (A) Representative whole-body red fluorescence image of a BALB/c mouse harboring a footpad infection of mCherry-*L. major*. (B) Red fluorescence intensity (top) and color photographs (bottom) of untreated mouse footpad infection after inoculation with 10^8 mCherry-*L. major* promastigotes. The fluorescence intensity scale bar applies to all footpad images and is given in arbitrary units.

Parasite activity screening and host cell toxicity. The antileishmanial activities of eight ZnDPA complexes were evaluated against *L. major* promastigotes (22). The inhibitory activity was determined using a CellTiter-Blue assay, which measures the ability of living cells to convert a redox dye (resazurin) into a fluorescent end product (resorufin) (see Fig. S5A in the supplemental material). The results in Fig. 3 show that all complexes were active against *L. major*, with EC_{50}s between 12.7 and 0.3 μM. In contrast, there was hardly any toxic effect against mammalian cells. Standard MTT assays (see Fig. S5B in the supplemental material) using Chinese hamster ovary (CHO) cells indicated that compounds 1, 4, 7, and 8 caused negligible toxicity up to 50 μM, whereas the other four complexes reduced cell viability ~30% at 50 μM. Although ZnDPA compound 7 was not the most active complex, it was chosen as the chemotherapeutic candidate for further evaluation against amastigotes and murine macrophages due to its structural simplicity and ease of production. The intracellular amastigote EC_{50}, measured using the back-transformation method, was ~5 μM, with a murine macrophage toxicity of >10 μM (Table 1). Histological analyses of uninfected mouse footpads treated with compound 7 were also performed to complement the *in vitro* toxicity results. After a 2-week treatment regimen of cutaneous footpad injections (see below), the mice were sacrificed and the footpads were harvested for hematoxylin-eosin staining and a vitality assessment. Compared to the control group injected with saline, no cellular or nuclear morphological changes in the cutaneous footpads were observed (see Fig. S6 in the supplemental material). Inflammatory foci that could indicate signs of cutaneous toxicity were not observed.

Cutaneous leishmaniasis BALB/c mouse model. A cutaneous leishmaniasis animal model was developed by inoculating cohorts of female BALB/c mice with stationary mCherry-*L. major* (10^8) in the left hind footpad (39). Lesion progression was monitored by imaging the red fluorescence emission of the mCherry-*L. major* amastigotes and also by measuring the thickness of inflamed footpads with a Vernier caliper. The cohorts were examined weekly for 5 weeks with a single cohort ($n = 4$) sacrificed every week for footpad harvesting and parasite counting. Figure 4 shows representative fluorescence images recorded weekly from infected mice.

A linear correlation was observed between fluorescence intensity and lesion size (Fig. 5A) and also fluorescence intensity and parasite burden in the footpad at each weekly time point (Fig. 5B). To prove that the red fluorescence at the site of infection was due to mCherry synthesis by the viable transgenic parasites, a control

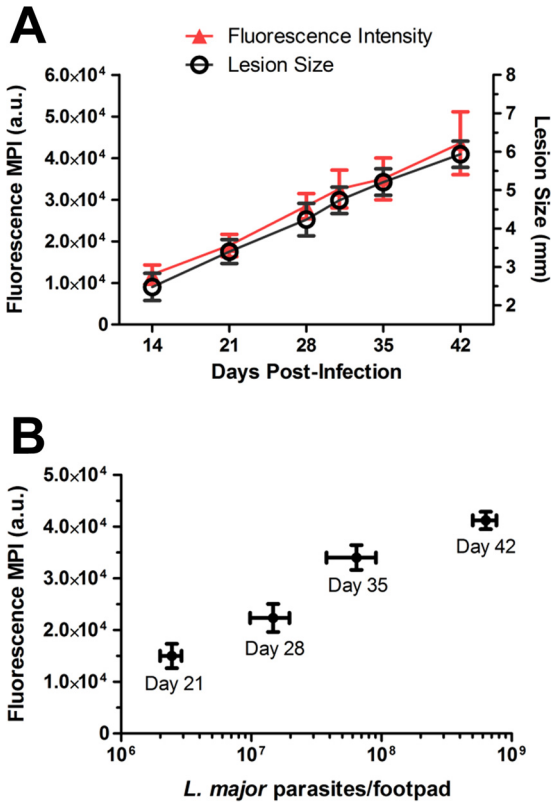

FIG 5 (A) Plot comparing red fluorescence mean pixel intensity (MPI) for infected mouse footpads in living mice (black) and footpad thickness (lesion size) (orange) over time. Each data point represents the means ± the standard errors ($n = 4$). (B) Plot of red fluorescence MPI for infected footpads in living mice and parasite counts in harvested footpads ($n = 4$). Each point represents means ± the standard errors.

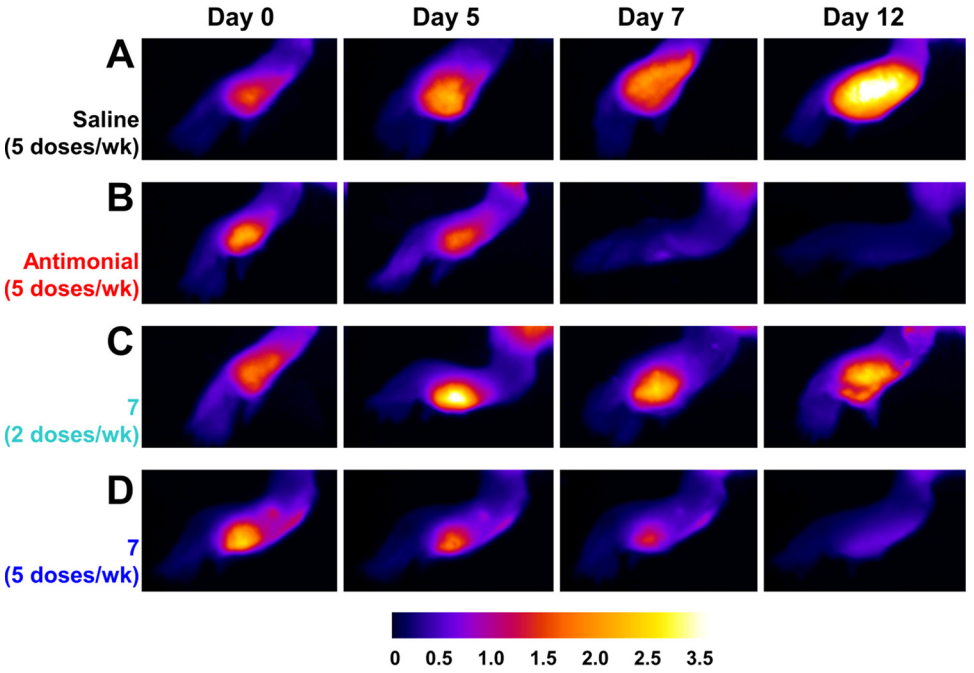

FIG 6 Representative red fluorescence intensity images of BALB/c mouse footpads after inoculation with mCherry-*L. major* promastigotes (10^8) and treated with saline at five doses/week (A), antimony(III) tartrate at five doses/week (B), and compound 7 at either two doses/week (C) or 5 doses/week (D) over a 12-day period. The mice were inoculated 14 days prior to the treatment start point (day 0). All doses were 30-μl intralesion injections of aqueous solutions containing saline (150 mM NaCl), antimony(III) tartrate (5.0 mg/kg), or compound 7 (0.1 mg/kg). The fluorescence intensity scale bar applies to all images and is given in arbitrary units.

experiment inoculated a separate cohort of mice with a *L. major* strain lacking the mCherry transcript and allowed infections to develop over 35 days. As expected, fluorescence imaging of the infection sites showed no measurable red fluorescence (see Fig. S7 in the supplemental material).

Treatment of cutaneous leishmaniasis model. The mouse leishmaniasis model described above was used with footpad infections of mCherry-*L. major*. Treatment efficacy experiments compared the antileishmanial activity of compound 7 to the standard agent potassium antimony(III) tartrate (antimonial) or no chemotherapeutic agent (saline) (5). Separate cohorts with 14-day footpad infections were given a daily intralesional injection of saline, compound 7 (0.1 mg/kg), or antimonial (5 mg/kg) for 5 days, followed by 2 days of recovery. An additional cohort was given two doses per week of compound 7 (0.1 mg/kg), followed by four recovery days. The red fluorescence emission from the cutaneous lesions was imaged four times over a 12-day period for all treatment regimens (Fig. 6).

Region-of-interest analysis of the fluorescence pixel intensity maps revealed a progressive loss in fluorescence in mice given compound 7 (five doses per week) compared to mice given saline (Fig. 7A). No significant decrease in *Leishmania* burden was observed in mice receiving only two weekly doses of compound 7. The diminished parasite burden was confirmed after dissection of the infected footpads and counting viable promastigotes differentiated from amastigotes after limiting dilution assay (Fig. 7B). The parasite burden was ~70% less in the cohort treated with five doses of compound 7 compared to saline-treated animals. In addition, the physical appearances of the treated footpads were significantly different at the conclusion of treatment (Fig. 7C). Antimonial treated footpads displayed cutaneous necrosis and scabbing, as expected (40). Conversely, footpads treated with compound 7 displayed some minor local inflammation but no obvious cutaneous reaction to the treatment.

DISCUSSION

Fluorescence microscopy with mSeek, a green-emitting fluorescent ZnDPA probe, found that ZnDPA has high affinity for *L. major* parasites. Confocal micrographs show diffuse internalization of the probe within the parasites colocalizing with the cytosolic mCherry reporter protein (Fig. 2; see also Fig. S2 and S3 in the supplemental material). The cytosolic distribution contrasts with that seen in planktonic bacteria, where mSeek localizes primarily in the bacterial envelope with no internalization (33). *In vitro* toxicity assays with eight different ZnDPA complexes revealed strong to moderate antileishmanial activity with minimal mammalian cell cytotoxicity (Fig. 3; see Fig. S5 in the supplemental material). Although ZnDPA compound 7 was not the most active complex, its structural simplicity and ease of production made it the most attractive choice for studies in the mouse footpad infection model. The ability to noninvasively monitor changes in the red fluorescence produced by the mCherry-*L. major* infections greatly facilitated the treatment efficacy experiments. Five weekly intralesional doses of compound 7 produced ~70% reduction in parasite burden compared to an untreated cohort (Fig. 5 to 7). The dose amount of compound 7 was ~50 times lower than the comparative dose of antimonial agent, and yet the reduction in infection burden was very similar over a 12-day period. Furthermore, treatment with compound 7 produced significantly less host tissue damage at the treatment site compared to antimonial treatment.

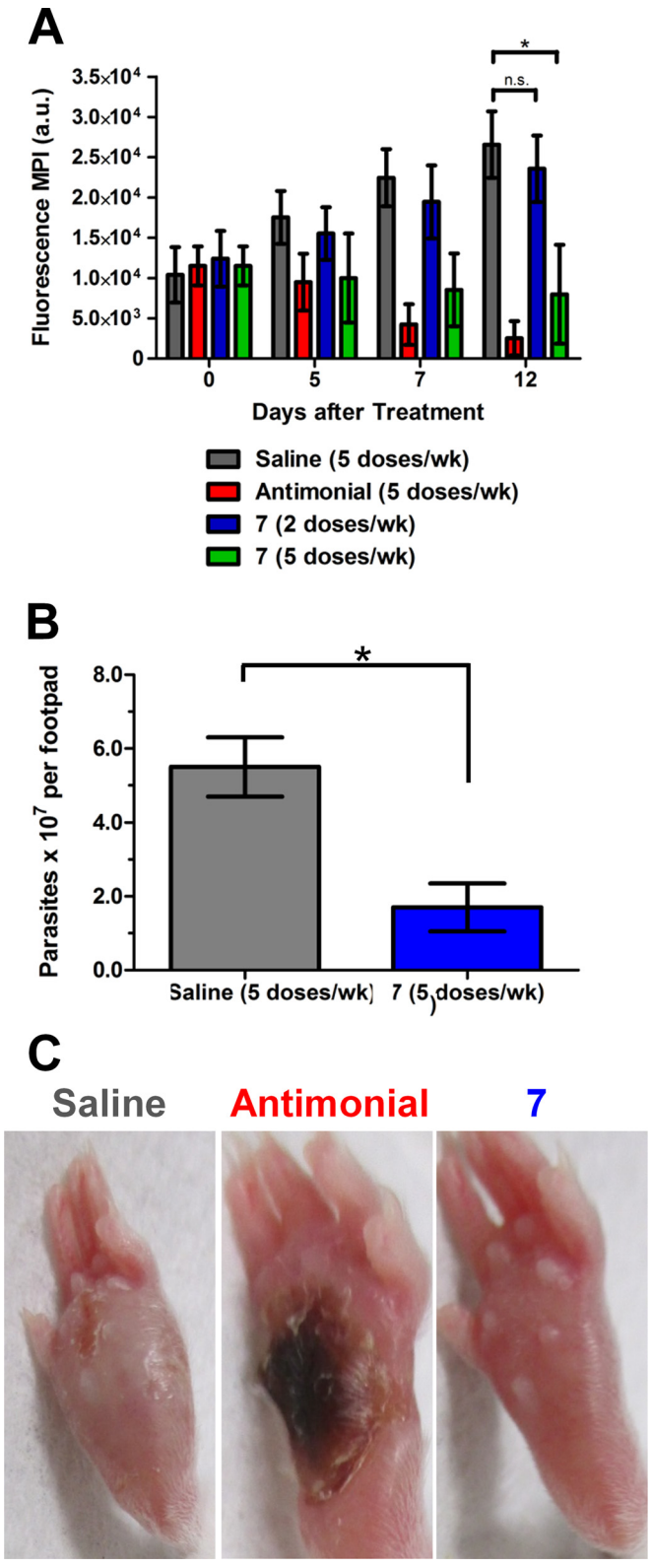

FIG 7 (A) Red fluorescence mean pixel intensities for separate treatment cohorts of living BALB/c mouse footpads infected with mCherry-*L. major* ($n = 4$). Each bar represents the means ± the standard errors. (B) Parasite counts in footpads harvested after 12-day treatments with saline treatment (gray) or compound 7 (blue). Bars represent the means ± the standard errors ($n = 3$). (C) Representative photographs of mouse footpads after 12 days of different treatments.

In vitro activity and toxicity measurements revealed that compound 7 is quite active against intracellular amastigotes and considerably less toxic against murine macrophages (Table 1). The high tolerance of the ZnDPA complex matches previous observations of no obvious acute murine toxicity (22, 27). However, more *in vivo* studies are needed to fully evaluate host toxicity and to more accurately measure the therapeutic window.

The mechanism of ZnDPA action against *L. major* is not presently clear and may be multifactorial. One possibility is that the ZnDPA complexes disrupt the parasite membrane. Alternatively, the ZnDPA complexes may alter metal cation concentrations within the cytosol. Zinc homeostasis is needed to maintain critical physiological processes (41, 42), and several studies report that *Leishmania* parasites are sensitive to doses of metal cations, including zinc, copper, and rhenium (43–47). Various zinc-sulfonamide complexes have low micromolar EC_{50}s against *L. major* and *L. amazonensis* (48-50), and a large screening study reported that various heterocyclic metal-binding compounds are highly active against *L. donovani* (51).

The World Health Organization has recommended combination therapy as a strategy to increase the therapeutic life span of drugs and delay the emergence of resistance (1). Thus, a question for future studies is whether ZnDPA coordination complexes can act in synergy with other therapeutic agents against cutaneous leishmaniasis. It is likely that ZnDPA complexes will have activity against other *Leishmania* species genetically similar to *L. major* and *L. donovani*, as well as against other trypanosomatids, including *Trypanosoma cruzi* (52–54). Another goal for future studies is to determine whether ZnDPA coordination complexes have activity against models of visceral Leishmaniasis. Fluorescent ZnDPA probes such as mSeek should be very helpful in determining systemic biodistribution, and we are encouraged by our previous work indicating that the biodistribution of ZnDPA probes is easily altered by rational structural modification (22–28).

ACKNOWLEDGMENTS

We thank M. Leevy and S. Chapman of the Notre Dame Integrated Imaging Facility for technical assistance with the imaging systems.

FUNDING INFORMATION

This work was funded in part by the Defense Threat Reduction Agency (grant HDTRA1-13-1-0016 to B.D.S.), the National Institutes of Health (NIH; grants R01GM059078 to B.D.S. and T32GM075762 to D.R.R.), the Indiana Clinical and Translational Institute funded by the NIH, National Center for Advancing Translational Science, Clinical and Translational Sciences Award, and the Eck Institute for Global Health (to M.A.M.).

REFERENCES

1. **World Health Organization.** 2012. Leishmaniasis. World Health Organization, Geneva, Switzerland. http://www.who.int/leishmaniasis/en/.
2. **Desjeux P.** 2001. The increase in risk factors for leishmaniasis worldwide. Trans R Soc Trop Med Hyg **95:**239–243. http://dx.doi.org/10.1016/s0035-9203(01)90223-8.
3. **Hartley MA, Drexler S, Ronet C, Beverley SM, Fasel N.** 2014. The immunological, environmental, and phylogenetic perpetrators of metastatic leishmaniasis. Trends Parasitol **30:**412–422. http://dx.doi.org/10.1016/j.pt.2014.05.006.
4. **Singh N, Kumar M, Singh RK.** 2012. Leishmaniasis: current status of available drugs and new potential drug targets. Asian Pac J Trop Med **5:**485–497. http://dx.doi.org/10.1016/S1995-7645(12)60084-4.
5. **Haldar AK, Sen P, Roy S.** 2011. Use of antimony in the treatment of leishmaniasis: current status and future directions. Mol Biol Int **2011:** 571242. http://dx.doi.org/10.4061/2011/571242.

6. **Machado-Pinto J, Pinto J, da Costa CA, Genaro O, Marques MJ, Modabber F, Mayrink W.** 2002. Immunochemotherapy for cutaneous leishmaniasis: a controlled trial using killed *Leishmania* (*Leishmania*) *amazonensis* vaccine plus antimonial. Int J Dermatol **41:**73–78. http://dx.doi.org/10.1046/j.1365-4362.2002.01336.x.
7. **Mishra M, Biswas UK, Jha DN, Khan AB.** 1992. Amphotericin versus pentamidine in antimony-unresponsive kala-azar. Lancet **340:**1256–1257. http://dx.doi.org/10.1016/0140-6736(92)92952-C.
8. **Dorlo TP, Balasegaram M, Beijnen JH, de Vries PJ.** 2012. Miltefosine: a review of its pharmacology and therapeutic efficacy in the treatment of leishmaniasis. J Antimicrob Chemother **67:**2576–2597. http://dx.doi.org/10.1093/jac/dks275.
9. **Wassef MK, Fioretti TB, Dwyer DM.** 1985. Lipid analyses of isolated surface membranes of *Leishmania donovani* promastigotes. Lipids **20:**108–115. http://dx.doi.org/10.1007/bf02534216.
10. **Wanderley JL, Thorpe PE, Barcinski MA, Soong L.** 2013. Phosphatidylserine exposure on the surface of *Leishmania amazonensis* amastigotes modulates in vivo infection and dendritic cell function. Parasite Immunol **35:**109–119. http://dx.doi.org/10.1111/pim.12019.
11. **Glew RH, Saha AK, Das S, Remaley AT.** 1988. Biochemistry of the *Leishmania* species. Microbiol Rev **52:**412–432.
12. **Turco SJ, Descoteaux A.** 1992. The lipophosphoglycan of *Leishmania* parasites. Annu Rev Microbiol **46:**65–94. http://dx.doi.org/10.1146/annurev.mi.46.100192.000433.
13. **Weingartner A, Kemmer G, Muller FD, Zampieri RA, Gonzaga dos Santos M, Schiller J, Pomorski TG.** 2012. Leishmania promastigotes lack phosphatidylserine but bind annexin V upon permeabilization or miltefosine treatment. PLoS One **7:**e42070. http://dx.doi.org/10.1371/journal.pone.0042070.
14. **Mendez-Samperio P, de la Rosa-Arana JL.** 2013. Antimicrobial peptides as parasiticidal against human trypanosomatids: mechanisms of action and current status in development. J Egypt Soc Parasitol **43:**195–208. http://dx.doi.org/10.12816/0006377.
15. **Dey T, Anam K, Afrin F, Ali N.** 2000. Antileishmanial activities of stearylamine-bearing liposomes. Antimicrob Agents Chemother **44:**1739–1742. http://dx.doi.org/10.1128/aac.44.6.1739-1742.2000.
16. **Afrin F, Dey T, Anam K, Ali N.** 2001. Leishmanicidal activity of stearylamine-bearing liposomes in vitro. J Parasitol **87:**188–193. http://dx.doi.org/10.1645/0022-3395(2001)087[0188:LAOSBL]2.0.CO;2.
17. **Rosypal AC, Hall JE, Bakunova S, Patrick DA, Bakunov S, Stephens CE, Kumar A, Boykin DW, Tidwell RR.** 2007. In vitro activity of dicationic compounds against a North American foxhound isolate of Leishmania infantum. Vet Parasitol **145:**207–216. http://dx.doi.org/10.1016/j.vetpar.2007.01.005.
18. **Loiseau PM, Cojean S, Schrevel J.** 2011. Sitamaquine as a putative antileishmanial drug candidate: from the mechanism of action to the risk of drug resistance. Parasite **18:**115–119. http://dx.doi.org/10.1051/parasite/2011182115.
19. **Hanshaw RG, Lakshmi C, Lambert TN, Smith BD.** 2005. Fluorescent detection of apoptotic cells using a zinc coordination complex with a selective affinity for membrane surfaces that are enriched in phosphatidylserine. Biophys J **88:**341a–341a. http://dx.doi.org/10.1002/cbic.200500149.
20. **Koulov AV, Stucker KA, Lakshmi C, Robinson JP, Smith BD.** 2003. Detection of apoptotic cells using a synthetic fluorescent sensor for membrane surfaces that contain phosphatidylserine. Cell Death Differ **10:**1357–1359. http://dx.doi.org/10.1038/sj.cdd.4401315.
21. **Lakshmi C, Hanshaw RG, Smith BD.** 2004. Fluorophore-linked zinc (II)dipicolylamine coordination complexes as sensors for phosphatidylserine-containing membranes. Tetrahedron **60:**11307–11315. http://dx.doi.org/10.1016/j.tet.2004.08.052.
22. **Plaunt AJ, Harmatys KM, Wolter WR, Suckow MA, Smith BD.** 2014. Library synthesis, screening, and discovery of modified zinc(II)-bis(dipicolylamine) probe for enhanced molecular imaging of cell death. Bioconjug Chem **25:**724–737. http://dx.doi.org/10.1021/bc500003x.
23. **Smith BA, Akers WJ, Leevy WM, Lampkins AJ, Xiao S, Wolter W, Suckow MA, Achilefu S, Smith BD.** 2010. Optical imaging of mammary and prostate tumors in living animals using a synthetic near infrared zinc (II)-dipicolylamine probe for anionic cell surfaces. J Am Chem Soc **132:**67–69. http://dx.doi.org/10.1021/ja908467y.
24. **Smith BA, Gammon ST, Xiao S, Wang W, Chapman S, McDermott R, Suckow MA, Johnson JR, Piwnica-Worms D, Gokel GW, Smith BD, Leevy WM.** 2011. In vivo optical imaging of acute cell death using a near-infrared fluorescent zinc-dipicolylamine probe. Mol Pharm **8:**583–590. http://dx.doi.org/10.1021/mp100395u.
25. **Smith BA, Harmatys KM, Xiao S, Cole EL, Plaunt AJ, Wolter W, Suckow MA, Smith BD.** 2013. Enhanced cell death imaging using multivalent zinc(II)-bis(dipicolylamine) fluorescent probes. Mol Pharm **10:**3296–3303. http://dx.doi.org/10.1021/mp300720k.
26. **Smith BA, Xie BW, van Beek ER, Que I, Blankevoort V, Xiao S, Cole EL, Hoehn M, Kaijzel EL, Lowik CW, Smith BD.** 2012. Multicolor fluorescence imaging of traumatic brain injury in a cryolesion mouse model. ACS Chem Neurosci **3:**530–537. http://dx.doi.org/10.1021/cn3000197.
27. **Leevy WM, Gammon ST, Jiang H, Johnson JR, Maxwell DJ, Jackson EN, Marquez M, Piwnica-Worms D, Smith BD.** 2006. Optical imaging of bacterial infection in living mice using a fluorescent near-infrared molecular probe. J Am Chem Soc **128:**16476–16477. http://dx.doi.org/10.1021/ja0665592.
28. **Leevy WM, Gammon ST, Johnson JR, Lampkins AJ, Jiang H, Marquez M, Piwnica-Worms D, Suckow MA, Smith BD.** 2008. Noninvasive optical imaging of staphylococcus aureus bacterial infection in living mice using a Bis-dipicolylamine-Zinc(II) affinity group conjugated to a near-infrared fluorophore. Bioconjug Chem **19:**686–692. http://dx.doi.org/10.1021/bc700376v.
29. **Leevy WM, Johnson JR, Lakshmi C, Morris J, Marquez M, Smith BD.** 2006. Selective recognition of bacterial membranes by zinc(II)-coordination complexes. Chem Commun http://dx.doi.org/10.1039/b517519d:1595-1597.
30. **Leevy WM, Serazin N, Smith BD.** 2007. Optical imaging of bacterial infection models. Drug Discov Today Dis Models **4:**91–97. http://dx.doi.org/10.1016/j.ddmod.2007.07.001.
31. **O'Neil EJ, Jiang H, Smith BD.** 2013. Effect of bridging anions on the structure and stability of phenoxide bridged zinc dipicolylamine coordination complexes. Supramol Chem **25:**315–322. http://dx.doi.org/10.1080/10610278.2013.776170.
32. **Xiao S, Abu-Esba L, Turkyilmaz S, White AG, Smith BD.** 2013. Multivalent dendritic molecules as broad spectrum bacteria agglutination agents. Theranostics **3:**658–666. http://dx.doi.org/10.7150/thno.6811.
33. **Rice DR, Gan H, Smith BD.** 2015. Bacterial imaging and photodynamic inactivation using zinc(II)-dipicolylamine BODIPY conjugates. Photochem Photobiol Sci **14:**1271–1281. http://dx.doi.org/10.1039/c5pp00100e.
34. **Desjeux P.** 2004. Leishmaniasis: current situation and new perspectives. Comp Immunol Microbiol Infect Dis **27:**305–318. http://dx.doi.org/10.1016/j.cimid.2004.03.004.
35. **Vacchina P, Morales MA.** 2014. In vitro screening test using Leishmania promastigotes stably expressing mCherry protein. Antimicrob Agents Chemother **58:**1825–1828. http://dx.doi.org/10.1128/AAC.02224-13.
36. **Hendrickx S, Boulet G, Mondelaers A, Dujardin JC, Rijal S, Lachaud L, Cos P, Delputte P, Maes L.** 2014. Experimental selection of paromomycin and miltefosine resistance in intracellular amastigotes of *Leishmania donovani* and *L. infantum*. Parasitol Res **113:**1875–1881. http://dx.doi.org/10.1007/s00436-014-3835-7.
37. **Titus RG, Marchand M, Boon T, Louis JA.** 1985. A limiting dilution assay for quantifying *Leishmania major* in tissues of infected mice. Parasite Immunol 7:545–555. http://dx.doi.org/10.1111/j.1365-3024.1985.tb00098.x.
38. **Goyard S, Segawa H, Gordon J, Showalter M, Duncan R, Turco SJ, Beverley SM.** 2003. An in vitro system for developmental and genetic studies of *Leishmania donovani* phosphoglycans. Mol Biochem Parasitol **130:**31–42.
39. **Calvo-Alvarez E, Guerrero NA, Alvarez-Velilla R, Prada CF, Requena JM, Punzon C, Llamas MA, Arevalo FJ, Rivas L, Fresno M, Perez-Pertejo Y, Balana-Fouce R, Reguera RM.** 2012. Appraisal of a *Leishmania major* strain stably expressing mCherry fluorescent protein for both in vitro and in vivo studies of potential drugs and vaccine against cutaneous leishmaniasis. PLoS Negl Trop Dis **6:**e1927. http://dx.doi.org/10.1371/journal.pntd.0001927.
40. **Oliveira LF, Schubach AO, Martins MM, Passos SL, Oliveira RV, Marzochi MC, Andrade CA.** 2011. Systematic review of the adverse effects of cutaneous leishmaniasis treatment in the new world. Acta Trop **118:**87–96. http://dx.doi.org/10.1016/j.actatropica.2011.02.007.
41. **Carvalho S, Barreira da Silva R, Shawki A, Castro H, Lamy M, Eide D, Costa V, Mackenzie B, Tomas AM.** 2015. LiZIP3 is a cellular zinc transporter that mediates the tightly regulated import of zinc in *Leishmania*

infantum parasites. Mol Microbiol **96:**581–595. http://dx.doi.org/10.1111/mmi.12957.
42. **Al-Mulla Hummadi YM, Al-Bashir NM, Najim RA.** 2005. The mechanism behind the antileishmanial effect of zinc sulfate. II. Effects on the enzymes of the parasites. Ann Trop Med Parasitol **99:**131–139. http://dx.doi.org/10.1179/136485905X19937.
43. **Sanchez-Delgado RA, Anzellotti A.** 2004. Metal complexes as chemotherapeutic agents against tropical diseases: trypanosomiasis, malaria, and leishmaniasis. Mini Rev Med Chem **4:**23–30. http://dx.doi.org/10.2174/1389557043487493.
44. **Ramirez-Macias I, Maldonado CR, Marin C, Olmo F, Gutierrez-Sanchez R, Rosales MJ, Quiros M, Salas JM, Sanchez-Moreno M.** 2012. In vitro anti-leishmania evaluation of nickel complexes with a triazolopyrimidine derivative against *Leishmania infantum* and *Leishmania braziliensis*. J Inorg Biochem **112:**1–9. http://dx.doi.org/10.1016/j.jinorgbio.2012.02.025.
45. **Caballero AB, Salas JM, Sanchez-Moreno M.** 2014. Metal-based therapeutics for leishmaniasis. *In* Leishmaniasis: trends in epidemiology, diagnosis, and treatment. InTech, Rijeka, Croatia. http://www.intechopen.com/books/leishmaniasis-trends-in-epidemiology-diagnosis-and-treatment/metal-based-therapeutics-for-leishmaniasis.
46. **Fattahi Bafghi A, Noorbala M, Noorbala MT, Aghabagheri M.** 2014. Anti-leishmanial effect of zinc sulphate on the viability of *Leishmania tropica* and *L. major* promastigotes. Jundishapur J Microbiol **7:**e11192. http://dx.doi.org/10.5812/jjm.11192.
47. **Najim RA, Sharquie KE, Farjou IB.** 1998. Zinc sulfate in the treatment of cutaneous leishmaniasis: an in vitro and animal study. Mem Inst Oswaldo Cruz **93:**831–837. http://dx.doi.org/10.1590/s0074-02761998000600025.
48. **Hassan Khan NU, Zaib S, Sultana K, Khan I, Mougang-Soume B, Nadeem H, Hassan M, Iqbal J.** 2015. Metal complexes of tosyl sulfonamides: design, X-ray structure, biological activities, and molecular docking studies. RSC Adv **5:**30125–30132. http://dx.doi.org/10.1039/c4ra16124f.
49. **da Silva LE, Joussef AC, Pacheco LK, da Silva DG, Steindel M, Rebelo RA, Schmidt B.** 2007. Synthesis and in vitro evaluation of leishmanicidal and trypanocidal activities of *N*-quinolin-8-yl-arylsulfonamides. Bioorg Med Chem **15:**7553–7560. http://dx.doi.org/10.1016/j.bmc.2007.09.007.
50. **da Silva LE, de Sousa PT, Maciel EN, Nunes RK, Eger I, Steindel M, Rebelo RA.** 2010. In vitro antiprotozoal evaluation of zinc and copper complexes based on sulfonamides containing 8-aminoquinoline ligands. Lett Drug Des Discov **7:**679–685. http://dx.doi.org/10.2174/157018010792929586.
51. **Pena I, Pilar-Manzano M, Cantizani J, Kessler A, Alonso-Padilla J, Bardera AI, Alvarez E, Colmenarejo G, Cotillo I, Roquero I, de Dios-Anton F, Barroso V, Rodriguez A, Gray DW, Navarro M, Kumar V, Sherstnev A, Drewry DH, Brown JR, Fiandor JM, Julio-Martin J.** 2015. New compound sets identified from high-throughput phenotypic screening against three kinetoplastid parasites: an open resource. Sci Rep **5:**8771. http://dx.doi.org/10.1038/srep08771.
52. **Zhang WW, Mendez S, Ghosh A, Myler P, Ivens A, Clos J, Sacks DL, Matlashewski G.** 2003. Comparison of the A2 gene locus in *Leishmania donovani* and *Leishmania major* and its control over cutaneous infection. J Biol Chem **278:**35508–35515. http://dx.doi.org/10.1074/jbc.M305030200.
53. **Rogers MB, Hilley JD, Dickens NJ, Wilkes J, Bates PA, Depledge DP, Harris D, Her Y, Herzyk P, Imamura H, Otto TD, Sanders M, Seeger K, Dujardin JC, Berriman M, Smith DF, Hertz-Fowler C, Mottram JC.** 2011. Chromosome and gene copy number variation allow major structural change between species and strains of *Leishmania*. Genome Res **21:**2129–2142. http://dx.doi.org/10.1101/gr.122945.111.
54. **Toledo A, Martın-Sánchez J, Pesson B, Sanchiz-Marın C, Morillas-Márquez F.** 2002. Genetic variability within the species *Leishmania infantum* by RAPD. A lack of correlation with zymodeme structure. Mol Biochem Parasitol **119:**257–264. http://dx.doi.org/10.1016/s0166-6851(01)00424-8.